Bull Mater Sci (2021)44:10
https://doi.org/10.1007/s12034-020-02302-4

Effects of TiO_2 phase and nanostructures as photoanode on the performance of dye-sensitized solar cells

MUQOYYANAH[1,2], A B SURIANI[1,2,*], A MOHAMED[1,3], N HASHIM[1,3], M H MAMAT[4], M K AHMAD[5], M H D OTHMAN[6], M A MOHAMED[7], M D NURHAFIZAH[8], M D BIROWOSUTO[9] and T SOGA[10]

[1]Nanotechnology Research Centre, Faculty of Science and Mathematics, Universiti Pendidikan Sultan Idris, 35900 Tanjung Malim, Malaysia
[2]Department of Physics, Faculty of Science and Mathematics, Universiti Pendidikan Sultan Idris, 35900 Tanjung Malim, Malaysia
[3]Department of Chemistry, Faculty of Science and Mathematics, Universiti Pendidikan Sultan Idris, 35900 Tanjung Malim, Malaysia
[4]NANO-ElecTronic Centre, Faculty of Electrical Engineering, Universiti Teknologi MARA, 40450 Shah Alam, Malaysia
[5]Microelectronic and Nanotechnology-Shamsuddin Research Centre, Faculty of Electrical and Electronic Engineering, Universiti Tun Hussein Onn Malaysia, 86400 Parit Raja, Malaysia
[6]Advanced Membrane Technology Research Centre, Universiti Teknologi Malaysia, 81310 Skudai, Malaysia
[7]Institute of Microengineering and Nanoelectronics, Universiti Kebangsaan Malaysia, 43600 Bangi, Selangor, Malaysia
[8]Nano-Optoelectronics Research and Technology Laboratory, School of Physics, Universiti Sains Malaysia, 11800 Minden Penang, Malaysia
[9]CNRS International NTU Thales Research Alliance, Research Techno Plaza, Singapore 637553, Singapore
[10]Department of Frontier Materials, Nagoya Institute of Technology, Nagoya 466-8555, Japan
*Author for correspondence (absuriani@yahoo.com)

MS received 9 July 2020; accepted 28 August 2020

Abstract. In this study, different titanium dioxide (TiO_2) nanostructures and phase were investigated as photoanode film for application in dye-sensitized solar cells. Rutile TiO_2 nanorods (NRs)-nanotrees (NTs) and TiO_2 NRs-microcauliflowers (MCFs) were synthesized via hydrothermal method for different time. The mixed phase of rutile-anatase film was fabricated by applying TiO_2 nanoparticles paste on the synthesized TiO_2 NRs-NTs via squeegee method. The counter electrode film was fabricated by spraying deposition and sputtering methods of reduced graphene oxide–multi-walled carbon nanotubes and platinum, respectively. Solar simulator measurement revealed that higher energy conversion efficiency (1.420%) and short-circuit current density (3.584 mA cm^{-2}) were achieved by using rutile TiO_2 NRs-MCFs film. The utilization of a thick rutile film with microparticle structures increases dye adsorption, and thus enhances the electron excitation.

Keywords. TiO_2; nanotrees; microcauliflowers; phase; efficiency; DSSCs.

1. Introduction

Dye-sensitized solar cells (DSSCs) have gained much interest as alternatives to conventional silicon-based solar cells because of their relatively high conversion efficiency (η) (14%) [1], simple fabrication and low production cost [2]. Several attempts have been made to improve the four components of DSSCs and enhance their performance and efficiency. These modifications include modifying the dye with metal complex, metal-free organic or natural material [3,4]; utilizing several electrolyte types (liquid, solid or quasisolid) [5]; and investigating several nanostructures and material for photoanode [6–9] and counter-electrode (CE) films [10–12]. Investigating the photoanode material and its nanostructures is important because of their crucial role in achieving a high DSSCs efficiency. Photoanode film needs to be considered because it provides the surface area for dye molecules adsorption, absorbs and scatters incident light and transfers the excited electrons to the substrate [13].

Wide-bandgap semiconductor materials, such as titanium dioxide (TiO_2) and zinc oxide (ZnO), are commonly used as photoanode films to maintain stability in a solution under irradiation [14]. ZnO precipitation has lower dye adsorption, which results in a lower DSSCs efficiency, because of its lower chemical stability after dye immersion [15]. TiO_2 offers high physical and chemical stabilities and a large surface area and is a potential solution for ZnO. The morphological properties of TiO_2 affect the performance of DSSCs. The 0-D and 1-D TiO_2 nanostructures offer their

Published online: 03 February 2021

own advantages and drawbacks for DSSCs application [8,16,17]. The combination of both structures enhances the performance of DSSCs compared with single structures [8,17]. Moreover, 3-D TiO_2 nanostructures have been widely investigated to further improve the performance of DSSCs. Zhao *et al* [18] demonstrated that applying TiO_2 hollow spheres on TiO_2 nanorods (NRs)-nanoflowers (NFs) achieved 7.5% efficiency compared with TiO_2 NRs-NFs (3.6%) or TiO_2 hollow spheres (5.48%) alone. Ahmad *et al* [9] showed that the utilization of TiO_2 NRs/micro-size flowers as photoanode film resulted in higher η (4.27%) compared with TiO_2 NRs (1.52%). This result is in a good agreement with the findings of Mary *et al* [19], who reported that rutile TiO_2 NFs enhance dye adsorption and thus improve the films' conductivity compared with TiO_2 NRs.

The crystalline phase of TiO_2 also affects DSSCs performance. Among the three crystalline phases of TiO_2, anatase and rutile phases are widely used because of their higher stability than brookite. Investigations on brookite phase as photoanode layer were conducted by modifying the TiO_2 nanostructures or the films' configuration. Xu *et al* [20] showed that pure brookite TiO_2 nanocubes (NC) have higher η (3.91%) than TiO_2 rice-like particles (0.35%). Their previous result showed that TiO_2 NC presented lower η (3.92%) compared with pure anatase TiO_2 nanoparticles (NPs; 7.13%). This lower η could be caused by the lower dye adsorption of TiO_2 NC because its large particles size affects the surface area. Furthermore, a higher η (8.83%) was achieved when TiO_2 NC was coated on TiO_2 NPs compared with pure brookite or anatase [21]. Recently, Peng *et al* [22] also investigated the brookite phase with different nanostructures and configurations as photoanode film in DSSCs and found that its efficiency is still lower than the anatase phase.

Mixed-phase rutile-anatase film presents higher η (7.1%) than pure rutile (4.4%) and anatase (5.8%) films [23]. Similar result was presented by Cao *et al* [8], who found that mixed-phase film has higher η (7.39%) than pure film (0.54 and 4.63% of pure rutile and anatase, respectively). Zheng *et al* [24] investigated TiO_2 nanofibre with different phases and showed that rutile and anatase phases have similar η (4.4 and 4.47%, respectively). Recently, Desai *et al* [25] also investigated different nanostructures of pure rutile films and found that the highest η was achieved by TiO_2 cauliflowers (14.21%) as photoanode film. In addition, different flower film morphologies affect the DSSCs performance. These results prove that the rutile phase can be used to substitute the common anatase phase as photoanode film.

The CE film, including type of material and its morphology, affects DSSCs performance. Based on the previous result, reduced graphene oxide (rGO) hybridized with multi-walled carbon nanotubes (MWCNTs) and platinum (Pt) NPs (TC14-rGO_MWCNTs/Pt) gives the highest η compared with other types of CE thin films [11]. Triple-tail sodium 1,4-bis(neopentyloxy)-3-(neopentyloxycarbonyl)-1,4-dioxobutane-2-sulphonate (TC14) can be used as surfactant for electrolyte preparation due to its effectiveness in optimizing and stabilizing the exfoliation process and producing TC14-rGO solution. The hybridization of these materials resulted in CE thin film with high conductivity due to its thin rGO layer and highly conductive MWCNTs and Pt NPs.

This research was carried out to investigate the effects of pure rutile and mixed-phase rutile-anatase photoanode films on the photovoltaic performance of DSSCs. Both rutile films were synthesized by hydrothermal method, which offers lower cost and simple preparation. The novelty of this research is the combination of the photoanode film (the absence of surfactant for rutile synthesis and bilayer photoanode fabricated by squeegee method) with the highly conductive CE thin film (TC14-rGO_MWCNTs/Pt).

2. Materials and methods

2.1 *Fabrication of photoanode films*

Pure rutile TiO_2 NRs-microcauliflowers (MCFs) were synthesized via two-step hydrothermal growth method with different solution recipes. The first hydrothermal solution to grow TiO_2 NRs was prepared according to a previous study [6,9,26]. In brief, 1:1 (v/v) of hydrochloric acid (HCl) and deionized (DI) water were mixed for approximately 5 min. Titanium butoxide (TBOT, 1:40) was added dropwise to the solution and stirred for 10 min until clear solution was observed. Clean fluorine-doped tin oxide (FTO) was placed upward in the autoclave. The prepared hydrothermal solution was then poured to the autoclave and placed into the electric oven for 5 h at 150°C. The synthesized TiO_2 NRs sample was dried at room temperature before performing the second hydrothermal process to synthesize TiO_2 MCFs. The second hydrothermal solution was prepared by following the methods of a previous study, but without using surfactant [9]. In brief, 1:1 (v/v) of HCl and DI water was mixed for about 5 min. TBOT (1:59) was added dropwise to the solution and stirred for 10 min until clear solution was observed. The second hydrothermal solution was then poured to the autoclave, which contained the synthesized TiO_2 NRs and subjected to the hydrothermal process for 2 h at 150°C. The sample was then collected, rinsed with DI water and annealed at 450°C for 30 min.

Rutile TiO_2 NRs-nanotrees (NTs) were synthesized following the TiO_2 NRs solution as mentioned previously. However, hydrothermal process of TiO_2 NRs-NTs was performed for 10 h. The mixed-phase rutile-anatase photoanode film was then fabricated by applying TiO_2 NPs paste as mentioned in previous studies [6,11,26]. In brief, titanium(IV) isopropoxide, titanium(IV) oxide and ethanol were mixed manually and sonicated for 5 min. The well-mixed paste was then applied to the synthesized TiO_2 NRs-NTs by

squeegee method. The prepared film was dried in an oven at 150°C for 10 min and then annealed at 450°C for 1 h.

2.2 *Fabrication of CE thin film*

TC14-rGO_MWCNTs/Pt CE thin film was fabricated via spraying deposition method of TC14-rGO_MWCNTs hybrid solution followed by sputtering Pt NPs as mentioned in previous studies [6,11]. The initial water-based GO solution was synthesized via electrochemical exfoliation utilizing triple-tail TC14 as surfactant. rGO was then produced by chemically reducing the synthesized GO by using hydrazine hydrate as reducing agent. The hybrid solution was prepared by mixing 1 wt% of MWCNTs synthesized from waste cooking palm oil to the produced TC14-rGO. The hybrid solution was sprayed to the preheated FTO with an airbrush at 10 cm distance and further annealed at 400°C for 1 h in the presence of argon gas. The fabricated hybrid film was then coated with 10 nm-thick Pt NPs using a sputter coater (Quorum Q150R S).

2.3 *Fabrication of DSSCs*

The fabricated photoanode films were immersed into 0.3 mM N719 dye for 24 h. The N719 powder was immersed into acetonitrile and 1-butanol (1:1, v/v) to prepare the dye solution. The photoanode and CE films were then assembled, and an electrolyte (1,2-dimethyl-3-propylimidazolium iodide) was poured in their gap.

The samples were characterized through field emission scanning electron microscopy (FESEM; Hitachi SU8020), electron dispersive X-ray spectroscopy (EDX; Horiba EMAX), X-ray diffractometry (XRD; Bruker D8 Advance), micro-Raman spectroscopy (Renishaw InVia microRaman System) and UV–visible (UV–Vis) spectrophotometry (Agilent Technologies Cary 60). DSSCs efficiency was measured using a solar simulator (Oriel Sol 1A) under 1 M solar illumination.

3. Results and discussion

3.1 *FESEM, EDX and HRTEM analysis*

The morphology of the synthesized TiO_2 NRs-MCFs determined by FESEM is shown in figure 1. As shown in figure 1a and b, the MCFs were spherical in shape and connect with each other. The average flower diameter varies from 3.73 to 4.39 µm (figure 1c). Moreover, the inset in figure 1d shows that the formed TiO_2 MCFs consist of NRs that are conglomerated with one another. The cross-section of TiO_2 NRs-MCFs show a very thick film with an average thickness of 102 µm (figure 1d). This thickness was dominated by MCFs structure, which were ∼18 times longer

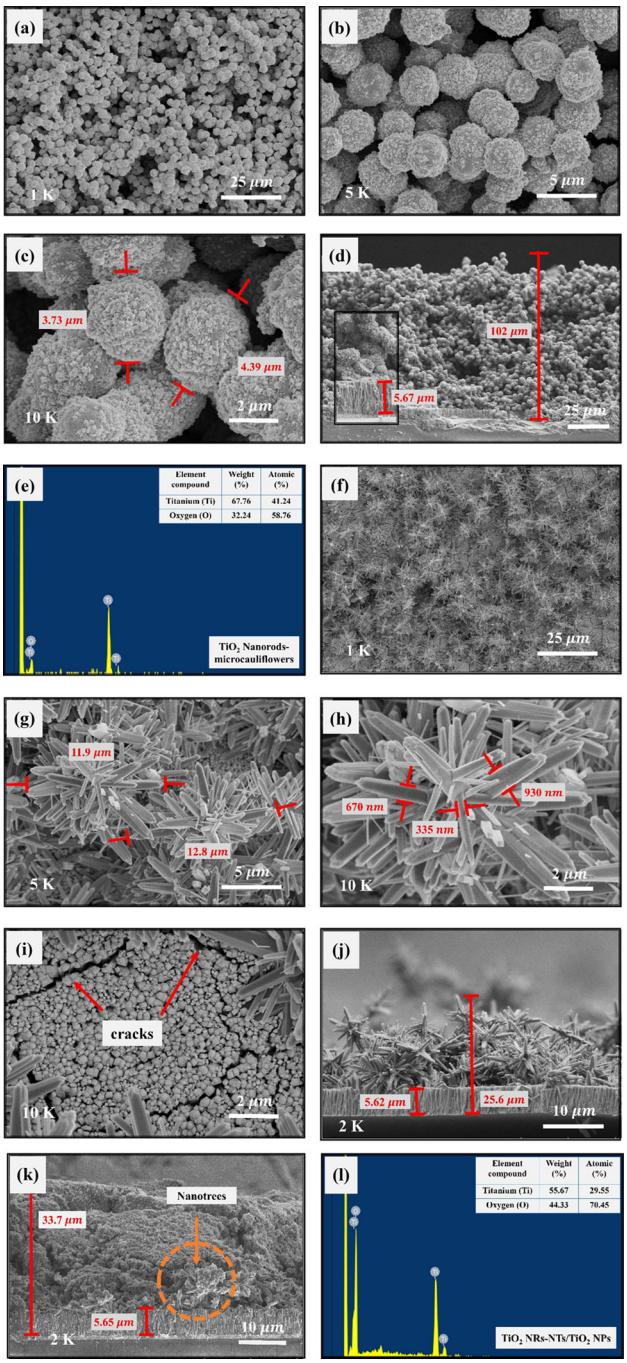

Figure 1. FESEM images and EDX spectra of the synthesized (**a–e**) TiO_2 NRs-MCFs and (**f–l**) TiO_2 NRs-NTs/TiO_2 NPs.

than the NRs in the bottom layer, because of the low acidity and concentration of the second hydrothermal solution. The absence of surfactant in the preparation of the second hydrothermal solution compared with the original work conducted by Ahmad *et al* [9] might affect the morphology and thickness and cause the rapid growth of MCFs. This result is in a good agreement with that of Liu and Aydil [27], who reported that the surfactant has a role in controlling and constraining the growth of nanostructures. The

inset in figure 1d also shows that the NRs produced are longer (5.67 μm) than the NRs synthesized for 5 h presented in the previous work [26]. The second step of the hydrothermal growth process makes the initially synthesized NRs to grow further [27]. EDX analysis (figure 1e) showed that the atomic percentage of Ti and O in the TiO_2 NRs-MCFs were 41.24 and 58.76%, respectively.

The morphology of the TiO_2 NRs-NTs as the bottom layer of the second photoanode film is shown in figure 1f–i. Figure 1f shows that many, almost uniform TiO_2 NTs grew on top of the TiO_2 NRs. The closer view of the TiO_2 NTs observed at 5 and 10 K magnifications shows that the formed TiO_2 NTs resemble a pine tree (figure 1g–h). The average tree diameter varied between 11.9 and 12.8 μm (figure 1g). The tree consists of many branches with varying diameters and lengths. The branches have a tetragonal crystal structure with a diameter that gradually decreased from the bottom to the tip (figure 1h). The facets of the branch are smooth, and its top is sharp. The diameter of the lower branches varies from 335 to 930 nm. Several branches were newly formed on the stem as shown by the small rods that look like a needle. Overall, the diameter of the NTs is ∼1.5 times longer compared with that of the NFs synthesized from 5 h of hydrothermal growth [26]. The longer length is possibly due to the longer duration of the synthesis, which allows abundant Ti^{4+} in the solution to fall and form trees. Meanwhile, the morphology of TiO_2 NRs at the bottom of NTs is similar to that of NRs synthesized for 5 h [6,26]. Dense and uniform NRs grew in the entire FTO substrate with diameter ranging from 87.3 to 325 nm. The NRs contain cracks that create a gap between the NRs (figure 1i), and these cracks were possibly caused by the longer synthesis time. The high heat caused by longer synthesis time results in high thermal stress, which triggers the cracks caused by the difference in the thermal expansion coefficients of the NRs and FTO substrate [28]. Furthermore, the length of the synthesized TiO_2 NRs is similar to that of TiO_2 NRs in the TiO_2 NRs-MCFs sample (5.62 μm) and ∼1.7 times longer than that of the NRs obtained from 5 h of synthesis [26]. A thicker film results from a longer synthesis time, which is in consistent with several reports [27,29]. Furthermore, the total thickness of the synthesized TiO_2 NRs-NTs was 25.6 μm as shown in figure 1j. The thickness of the final photoanode film was ∼33.7 μm after applying TiO_2 NPs on TiO_2 NRs-NTs (figure 1k). A big NTs shown by the orange circle was also covered with NPs. In addition, the thickness of the TiO_2 NRs (5.65 μm) was consistent with the pure TiO_2 NRs-NTs. Meanwhile, the size of TiO_2 NPs as the second layer of the mixed-phase photoanode layer was similar to the previous results, which were in the range of ∼25 nm [6,11,26]. EDX analysis (figure 1l) showed that the atomic percentage of Ti and O in TiO_2 NRs-NTs/TiO_2 NPs were 29.55 and 70.45%, respectively.

3.2 *Micro-Raman spectroscopy*

The micro-Raman spectra of the synthesized pure rutile TiO_2 NRs-MCFs and TiO_2 NRs-NTs are presented in figure 2. Both samples presented two intense peaks at 448 and 447 cm^{-1} and at 615 and 609 cm^{-1}, which correspond to the E_g and A_{1g} modes, respectively. These peaks were resulted from O–Ti–O symmetric stretching vibration and anti-symmetric bending vibration. A weak sharp peak located at 100–150 cm^{-1} correspond to the B_{1g} mode resulted from O–Ti–O symmetric bending vibration [30]. These three peaks further confirmed that the synthesized samples were in the rutile phase, which is presented by three Raman active modes expressed as $A_{1g} + B_{1g} + E_g$ [31–33]. Another broad peak observed at 242 and 239 cm^{-1} was caused by multiple phonon scattering, which indicates the nanometre scale of the synthesized samples. In addition, a small bump peak observed at 696 cm^{-1} resulted from the existence of NTs [33].

3.3 *XRD analysis*

The crystallinity of the fabricated photoanode films were investigated by XRD and the results are presented in figure 3. The bottom graph shows that the TiO_2 NRs-MCFs

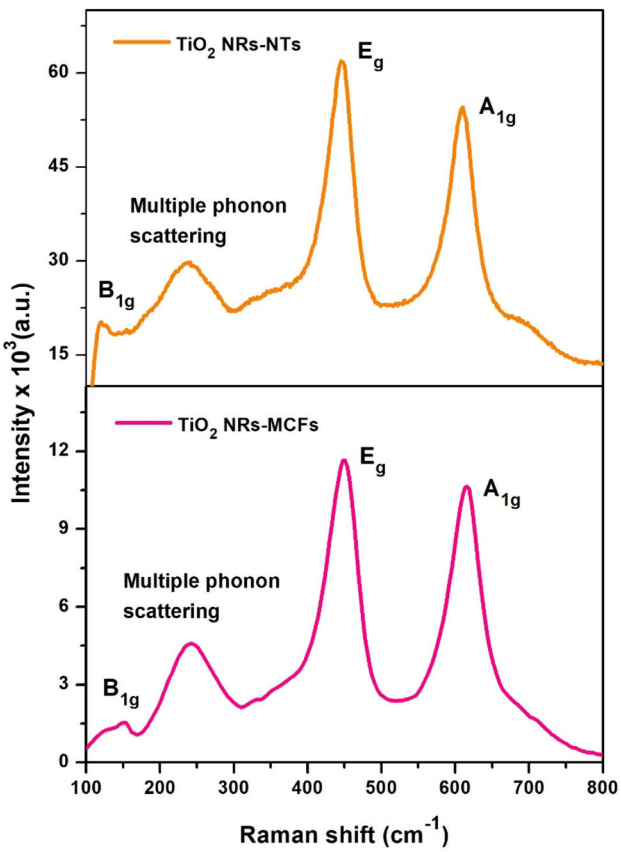

Figure 2. Micro-Raman spectra of the synthesized TiO_2 NRs-MCFs and TiO_2 NRs-NTs.

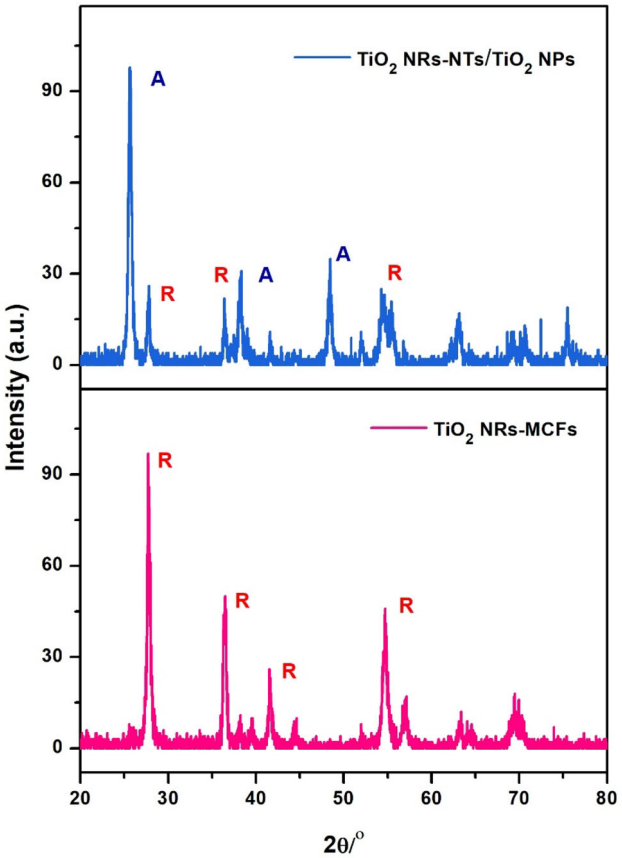

Figure 3. XRD pattern of the fabricated photoanode films.

presented four intense peaks located at 27.83, 36.49, 41.75 and 55.07°, which correspond to the [110], [101], [111] and [301] planes, respectively. These peaks further confirmed that the synthesized TiO_2 NRs-MCFs were in the pure rutile phase (PDF No. 01-071-4809). The most intense peak at 27.83° was regarded as the most thermodynamically stable plane because of its faster growth rate than the other planes [34]. The top graph shows the additional peaks that represent the anatase phase. This graph confirmed that the fabricated TiO_2 NRs-NTs/TiO_2 NPs was in the mixed rutile-anatase phase. These additional anatase intense peaks were located at 25.65, 38.97 and 48.38°, which correspond to the [101], [004] and [200] planes, respectively (PDF No. 01-075-1537). The intensity of the rutile peaks in the top graph was lower compared with that in the bottom graph. This difference was probably caused by the thick TiO_2 NPs coated on top of the TiO_2 NRs-NTs, and the TiO_2 NPs affected laser penetration.

Overall, the sharp and high peak intensities observed in both samples further confirmed that the fabricated photoanode films possessed a strong crystallinity, as confirmed by crystallinity measurement. The films' crystallite percentages were over 80%. TiO_2 NRs-NTs/TiO_2 NPs had lower crystallinity percentage (83.2%) than TiO_2 NRs-MCFs (86.1%) because of its higher porosity obtained from the coated TiO_2 NPs (rutile-anatase crystallite percentage ratio; 26.6:73.4%) [6]. Based on table 1, TiO_2 NRs-MCFs had small crystallite size (17.1–22.9 nm) with high crystallite peak percentage (over 85%). The pure anatase crystallite on TiO_2 NRs-NTs/TiO_2 NPs sample also presented a small crystallite percentage (18.8–22.2 nm).

3.4 *UV–Vis spectrophotometry*

The transmittance value of the fabricated photoanode films was measured using a UV–Vis spectrophotometer, and the results are presented in figure 4a. The highest transmittance value was presented by TiO_2 NRs-NTs (0.63%), because this film was the thinnest among the films. This value was decreased to 0.34% after the addition of TiO_2 NPs to the upper layer of the photoanode film. The homogeneous thick TiO_2 NPs in the coating were highly interconnected towards each other. Meanwhile, TiO_2 NRs-MCFs exhibited the lowest transmittance value of 0.24%, because this film was the thickest among the films (see FESEM images). Bandgap energy (E_g) measurement was performed based on Tauc's plot from the transmittance value, and the results are presented in figure 4b. Pure rutile TiO_2 NRs-MCFs and the photoanode's bottom layer composed of TiO_2 NRs-NTs had

Table 1. Crystallite size and its percentage of the selected peaks of the fabricated photoanode films.

Photoanode film	Peak (°)	Film's crystallite percentage (%)	Crystallite percentage (%)	Crystallite size (nm)
TiO_2 NRs-MCFs	26–29	86.1	88.4	20.2
	35–37.5		95	19.2
	40.5–43		93.7	22.9
	53.5–56		87.3	17.1
TiO_2 NRs-NTs/TiO_2 NPs	24–27	83.2;	91.5	18.8
	27–29	26.6 Rutile	83.4	25.2
	37–39	73.4 Anatase	75.1	23.6
	47–50		91	22.2
	53.5–55		79.9	93.3
	55–56		83.2	49.9
	61.5–64		75.6	28.1

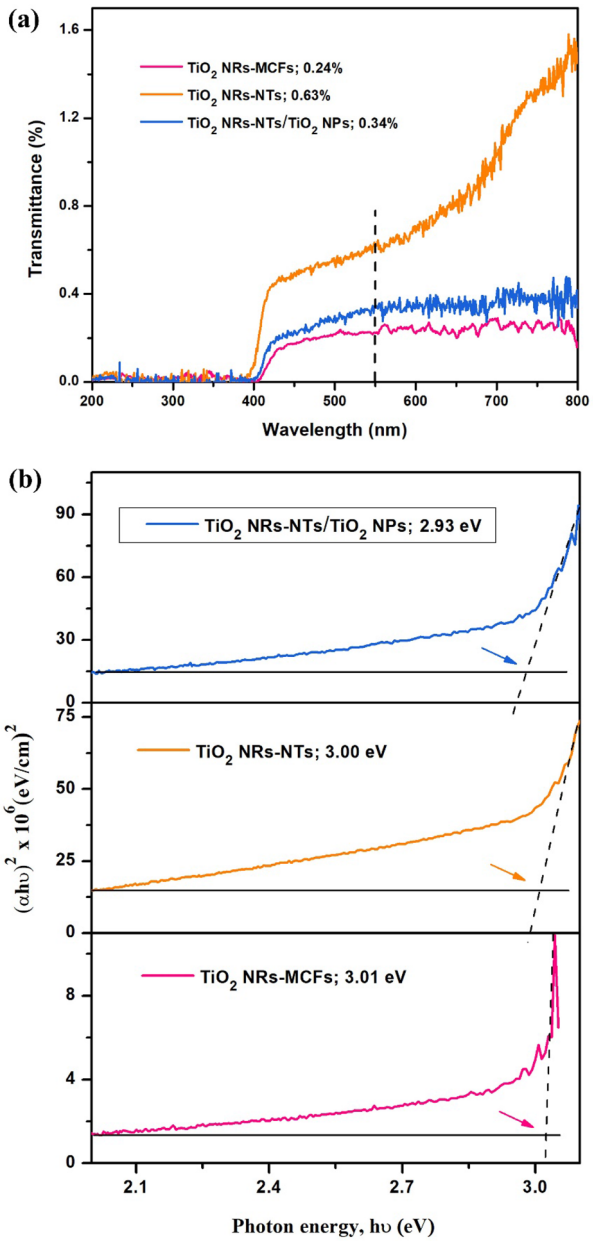

Figure 4. (**a**) Transmittance value and (**b**) E_g measurement of the fabricated photoanode films.

Table 2. Transmittance and E_g value of the fabricated photoanode films.

Photoanode film	Transmittance (%)	E_g value (eV)
TiO_2 NRs-MCFs	0.24	3.01
TiO_2 NRs-NTs	0.63	3.00
TiO_2 NRs-NTs/TiO_2 NPs	0.34	2.93

E_g value of 3.01 and 3.00 eV, respectively, which were in a good agreement with the theory [35]. The E_g value after TiO_2 NPs were coated on TiO_2 NRs-NTs decreased to 2.93 eV. This finding suggested that electron transfer is better and faster through mixed-phase film than single or pure phase film [6,11,26]. The closely stacked TiO_2 NRs-NTs and TiO_2 NPs showed a synergetic effect; thus, the E_g value of the mixed-phase film decreased [36]. The transmittance and E_g values of the fabricated photoanode films are summarized in table 2.

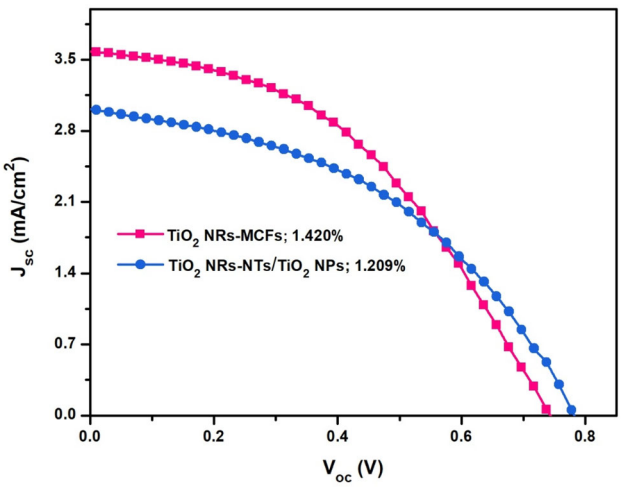

Figure 5. Solar simulator measurement of DSSCs with TiO_2 NRs-MCFs and TiO_2 NRs-NTs/TiO_2 NPs as photoanode films.

3.5 *Solar simulator measurement*

The photovoltaic performance of the DSSCs based on TiO_2 NRs-MCFs and TiO_2 NRs-NTs/TiO_2 NPs as photoanode films and TC14-rGO_MWCNTs/Pt as CE film are presented in figure 5. Based on graph, DSSCs with TiO_2 NRs-MCFs presented higher η (1.420%) compared with TiO_2 NRs-NTs/TiO_2 NPs (1.209%). The higher short-circuit current density (J_{sc}) of pure rutile TiO_2 NRs-MCFs (3.584 mA cm^{-2}) was possibly due to the thick layer of TiO_2 MCFs as the second layer of the photoanode, because the lengths of the TiO_2 NRs in both samples were similar (refer figure 1d and k). The vertically aligned TiO_2 NRs as the photoanode's bottom layer for the fabricated films accelerate electrons transfer from the upper layer to complete the electrons cycle in DSSCs device [11,23,26]. However, thicker layer of 3-D TiO_2 MCFs offered a large surface area for dye adsorption, thereby enhancing electrons excitation. This occurrence was in a good agreement with the study of Desai *et al* [25]. The morphology of TiO_2 MCFs consists of TiO_2 NRs that conglomerated with each other accelerated the excitation of electrons between the MCFs. The electrons were further transferred to the TiO_2 NRs in the bottom layer of the photoanode. In addition, the photogenerated electrons loss can be minimized because of the flowery structure [25]. By contrast, the thinner TiO_2 NPs layer resulted in lower dye adsorption, which affected the excited electrons. This mechanism was supported by the fact that anatase 0-D TiO_2

Table 3. DSSCs photovoltaic performance based on TiO_2 NRs-MCFs and TiO_2 NRs-NTs/TiO_2 NPs as photoanode films.

Photoanode film	η (%)	V_{oc} (V)	J_{sc} (mA cm^{-2})	FF
TiO_2 NRs-MCFs	1.420	0.749	3.584	44.5
TiO_2 NRs-NTs/TiO_2 NPs	1.209	0.782	3.020	44.0

NPs presented slower electrons transport (the electrons moved by hopping from one particle to another) compared with rutile 1-D TiO_2 NRs (the electrons moved directly in a straight line) [17,37–39].

On the other hand, mixed-phase rutile-anatase TiO_2 NRs-NTs/TiO_2 NPs presented higher open-circuit voltage (V_{oc}; 0.782 V) compared with pure rutile TiO_2 NRs-MCFs (0.749 V). A higher V_{oc} suggests a lower charge recombination and fewer defects [40]. The thinner TiO_2 NPs layer on TiO_2 NRs-NTs/TiO_2 NPs sample and its closely interconnected TiO_2 NPs particles [6,11,26] resulted in lower charge recombination than TiO_2 NRs-MCFs. The branches of TiO_2 NTs also acted as electrons transporter that transferred the excited electrons from TiO_2 NPs via branch-to-branch heterostructures [34]. This was also supported by the lower E_g value of two layer TiO_2 NRs-NTs/TiO_2 NPs photoanode that accelerated the electrons movement (to the photoanode substrate and further to the CE film to complete one cycle of DSSCs process) and prevented the electron recombination [17]. As a consequence, longer electron lifetime was achieved caused by the prevention of those electron recombination [41]. By contrast, the loose morphology of TiO_2 MCFs, as presented in the FESEM images (refer figure 1a–d), might have increased the defects number of the fabricated photoanode film, which resulted in a lower V_{oc} value compared with that of TiO_2 NRs-NTs/TiO_2 NPs. In addition, the thicker TiO_2 MCFs layer as compared with TiO_2 NPs gives more drawbacks in term of high electrons recombination rates [17,42]. The morphology of the CE thin film also affected the photovoltaic performance of the DSSCs. The thin and non-agglomerated TC14-rGO layer accelerates the electron transfer through the film and is further supported by the loose MWCNTs structure that decreases the internal resistance [43]. The summary of the solar simulator measurement for the photoanode films is presented in table 3.

4. Conclusions

Pure rutile TiO_2 NRs-MCFs and mixed-phase rutile-anatase TiO_2 NRs-NTs/TiO_2 NPs were successfully fabricated via simple hydrothermal and squeegee methods. The DSSCs with TiO_2 NRs-MCFs had higher η (1.420%) and higher J_{sc} (3.584 mA cm^{-2}) than the DSSCs with TiO_2 NRs-NTs/TiO_2 NPs. TiO_2 MCFs with microparticle structure were thicker, which increased the dye adsorption and enhanced the electrons excitation, compared with TiO_2 NRs-NTs/TiO_2 NPs. In addition, the vertically aligned TiO_2 NRs as the bottom layer of the photoanode accelerated the electrons transfer, which resulted in the high J_{sc} value. Hence, higher dye adsorption can be obtained by using the thick and spherical morphology of pure rutile TiO_2 film compared with anatase TiO_2 film.

Acknowledgements

We would like to express our appreciation to the Fundamental Research Grant Scheme (Grant Code: 2015-0154-102-02) for the financial support.

References

[1] Kakiage K, Aoyama Y, Yano T, Oya K, Fujisawa J and Hanaya M 2015 *Chem. Commun.* **51** 15894
[2] O'Regan B and Grätzel M 1991 *Nature* **353** 737
[3] Calogero G, Bartolotta A, Marco G D, Carlo A D and Bonaccorso F 2015 *Chem. Soc. Rev.* **44** 3244
[4] Mehmood U, Malaibari Z, Rabani F A, Rehman A U, Ahmad S H A, Atieh M A *et al* 2016 *Electrochim. Acta* **203** 162
[5] Mehmood U, Rahman S, Harrabi K, Hussein I A and Reddy B V S 2014 *Adv. Mater. Sci. Eng.* **2014** 1
[6] Suriani A B, Muqoyyanah, Mohamed A, Mamat M H, Othman M H D, Ahmad M K *et al* 2019 *Nano-Struct. Nano-Objects* **18** 100314
[7] Xie Y, Zhou X, Mi H, Ma J, Yang J and Cheng J 2018 *Appl. Surf. Sci.* **434** 1144
[8] Cao Y, Li Z, Wang Y, Zhang T, Li Y, Liu X *et al* 2016 *J. Electron. Mater.* **45** 4989
[9] Ahmad M K, Mohan V M and Murakami K 2015 *J. Sol-Gel Sci. Technol.* **73** 655
[10] Guai G H, Song Q L, Guo C X, Lu Z S, Chen T, Ng C M *et al* 2012 *Sol. Energy* **86** 2041
[11] Suriani A B, Muqoyyanah, Mohamed A, Othman M H D, Mamat M H, Hashim N *et al* 2018 *J. Mater. Sci.: Mater. Electron.* **29** 10723
[12] Popoola I K, Gondal M A, Alghamdi J M and Qahtan T F 2018 *Sci. Rep.* **8** 12864
[13] Kim S B, Park J Y, Kim C S, Okuyama K, Lee S E, Jang H D *et al* 2015 *J. Phys. Chem. C* **119** 16552
[14] Luque A and Hegedus S 2011 (second) *Handbook of photovoltaic science and engineering* (United Kingdom: John Wiley & Sons, Ltd.)
[15] Quintana M, Edvinsson T, Hagfeldt A and Boschloo G 2007 *J. Phys. Chem. C* **111** 1035
[16] Wang J, Qu S, Zhong Z, Wang S, Liu K and Hu A 2014 *Prog. Nat. Sci.: Mater. Int.* **24** 588
[17] Wu W, Liao J, Chen H, Yu X, Su C and Kuang D 2012 *J. Mater. Chem.* **22** 18057
[18] Zhao P, Cheng P, Wang B, Yao S, Sun P, Liu F *et al* 2014 *RSC Adv.* **4** 64737
[19] Mary J S S, Princy P, Steffy J A J, Kumar P N, Bachan N and Shyla J M 2016 *Int. J. Tech. Res. Appl.* **37** 60

[20] Xu J, Wu S, Ri J H, Jin J and Peng T 2016 *J. Power Sources* **327** 77
[21] Xu J, Li K, Wu S, Shi W and Peng T 2015 *J. Mater. Chem. A* **3** 7453
[22] Peng T, Xu J and Chen R 2020 *Chem. Phys. Lett.* **738** 136902
[23] Hafez H, Lan Z, Li Q and Wu J 2010 *Nanotechnol. Sci. Appl.* **3** 45
[24] Zheng D, Xiong J, Guo P, Li Y and Gu H 2016 *J. Nanosci. Nanotechnol.* **16** 613
[25] Desai N D, Khot K V, Dongale T, Musselman K P and Bhosale P N 2019 *J. Alloys Compd.* **790** 1001
[26] Suriani A B, Muqoyyanah, Mohamed A, Mamat M H, Hashim N, Isa I M *et al* 2018 *Opt. - Int. J. Light Electron Opt.* **158** 522
[27] Liu B and Aydil E S 2009 *J. Am. Chem. Soc.* **131** 3985
[28] Meng L, Li C and Dos Santos M P 2011 *J. Inorg. Organomet. Polym. Mater.* **21** 770
[29] Ahmad M K and Murakami K 2015 *Appl. Mech. Mater.* **773–774** 725
[30] Yan J, Wu G, Guan N, Li L, Li Z and Cao X 2013 *Phys. Chem. Chem. Phys.* **15** 10978
[31] Luo Z, Poyraz A S, Kuo C, Miao R, Meng Y, Chen S *et al* 2015 *Chem. Mater.* **27** 6
[32] Meier R J 2005 *Chem. Soc. Rev.* **34** 743
[33] Ahmad M K, Mokhtar S M, Soon C F, Nafarizal N, Suriani A B, Mohamed A *et al* 2016 *J. Mater. Sci.: Mater. Electron.* **27** 7920
[34] Zhou W, Liu X, Cui J, Liu D, Li J, Jiang H *et al* 2011 *CrystEngComm* **13** 4557
[35] Lei J, Li H, Zhang J and Anpo M 2016 in *Low-dimensional and nanostructured materials and devices* H Ūnlū *et al* (eds) (Switzerland: Springer) p 423
[36] Wu C, Yue Y, Deng X, Hua W and Gao Z 2004 *Catal. Today* **93–95** 863
[37] Jiang W, Liu H, Yin L, Shi Y, Chen B, Jiang W *et al* 2015 *Electrochim. Acta* **176** 1036
[38] Wang H, Bai Y, Wu Q, Zhou W, Zhang H, Li J *et al* 2011 *Phys. Chem. Chem. Phys.* **13** 7008
[39] Kosyachenko L (ed) 2011 *Solar cell: dye-sensitized devices* (Croatia: InTech) p 192
[40] Keshavarzi R, Mirkhani V, Moghadam M, Tangestaninejad S and Mohammadpoor-Baltork M 2015 *Langmuir* **31** 11659
[41] Dahlan D, Md Saad S K, Berli A U, Bajili A and Umar A A 2017 *Physica E* **91** 185
[42] Tsai J K, Hsu W D, Wu T C, Meen T H and Chong W J 2013 *Nanoscale Res. Lett.* **8** 1
[43] Hwang S, Batmunkh M, Nine M J, Chung H and Jeong H 2015 *Chem. Phys. Chem.* **16** 53